Chemical Engineering Journal 518 (2025) 164654

Contents lists available at ScienceDirect

Chemical Engineering Journal

journal homepage: www.elsevier.com/locate/cej

# Cerium silicate formation in solid oxide electrolysis cells: Effects on durability and mitigation strategies

Matthias Riegraf [a,*], Alexander Surrey [b], Noriko Sata [a], Rémi Costa [a]

[a] German Aerospace Centre (DLR), Institute of Engineering Thermodynamics, Pfaffenwaldring 38-40, 70569 Stuttgart, Germany
[b] Sunfire AG, Gasanstaltstraße 2, 01237, Dresden, Germany

ARTICLE INFO

*Keywords:*
Co-electrolysis
Steam electrolysis
Ni/gadolinium-doped ceria
SOEL
SOEC

ABSTRACT

High-temperature solid oxide electrolysis (SOEL) exhibits superior electrical efficiencies compared to low-temperature electrolysis technologies and possess the unique ability to produce syngas via simultaneous co-electrolysis of steam and carbon dioxide. However, impurity-induced degradation can significantly reduce their lifetime and the requirements for feed gas quality remain unclear. This study presents the first systematic investigation of silicate formation in state-of-the-art Ni/Gadolinium-doped ceria (CGO) fuel electrodes and its severe degradation impact, an issue addressed in multiple German research projects by DLR and Sunfire. Through microstructural and crystallographic analyses, the formation of the cerium silicate phase $Ce_{4.67}(SiO_4)_3O$ predominantly at the electrolyte|electrode interface is established. A progressive macroscopic color change along the channel is demonstrated to be a reliable indicator for cerium silicate formation. Water quality is identified as a critical factor for minimizing degradation rates. At 860 °C, degradation rates of 10.4–14.8 mΩ $cm^2$/kh were observed in single cells operated in co-electrolysis with ultrapure water containing <1 ppb silica, while reverse osmosis water with >40 ppb silica led to a 3-5× acceleration in degradation. The results reveal a highly detrimental solid oxide electrolysis cell (SOEC) degradation mechanism and underscore the necessity of stringent feed water purity to ensure stable long-term stability and commercial viability.

## 1. Introduction

The decarbonization of energy-intensive industries is critical to mitigating climate change, and electrification through power-to-X (PtX) technologies presents a promising pathway to achieve this goal via sector coupling. PtX concepts can utilize renewable energy, water, and captured carbon dioxide to synthesize commodity chemicals and e-fuels with a reduced carbon footprint [1]. A key enabler for the widespread adoption of PtX processes is the development of efficient and cost-effective electrolysis technologies.

Among the different water electrolysis technologies, high-temperature solid oxide electrolysis (SOEL) stands out for its superior electrical efficiency, owing to its kinetic and thermodynamic advantages [2]. Furthermore, solid oxide cells (SOCs) have the unique benefit of being able to operate in co-electrolysis of $CO_2$ and $H_2O$ generating tailor-made syngas ratios in one reactor which can be directly coupled with downstream chemical processes. These downstream processes, such as methanol synthesis, Fischer-Tropsch synthesis and methanation are typically exothermic, creating synergies with SOEL by providing the large amounts of waste heat required for steam generation which can boost electrical SOEL system efficiencies by >10 % [3]. For example, thermal integration between co-electrolysis and catalytic methanation allows unrivaled power-to-methane efficiencies exceeding 80 $\%_{LHV}$ [4].

For SOEL to achieve commercial viability, long-term operational reliability is crucial, driving significant research into mitigating degradation in cells and stacks. Degradation rates as low as 0.5 % per 1000 h are targeted by the Strategic Research & Innovation Agenda from the Clean Hydrogen Joint Undertaking by 2030 [5]. Such degradation rates have already been achieved in steam electrolysis for operating times >1000 h [6–12]. However, fewer studies have focused on the durability of state-of-the-art SOCs in co-electrolysis operation [9,13].

Degradation in SOCs results from both intrinsic and extrinsic mechanisms, and dominant degradation mechanisms are now frequently the effect of external impurities rather than the internal effects of high-temperature diffusion processes [14]. State-of-the-art Ni/cermet fuel electrodes show degradation upon exposure to Ni surface deactivation from sulfur contaminants and carbon formation [15,16]. Ni/Gadolinia-doped ceria (CGO) fuel electrodes typically used in

* Corresponding author.
*E-mail address:* Matthias.Riegraf@dlr.de (M. Riegraf).

https://doi.org/10.1016/j.cej.2025.164654
Received 4 April 2025; Received in revised form 14 May 2025; Accepted 7 June 2025
Available online 10 June 2025

electrolyte-supported cells (ESCs) and metal-supported cells (MSCs), show higher tolerance towards both sulfur poisoning and coking compared to Ni/Yttria-stabilized zirconia (YSZ) [17,18], which are preferred in fuel electrode supported cell architectures due to their high mechanical stability. Ni/YSZ fuel electrodes were also reported to suffer from $SiO_2$ deposition during electrolysis [19], with silica hypothesized to play a role during Ni migration which is one of the most detrimental degradation mechanisms in Ni/YSZ electrodes [20]. Potential sources of silica include steel pipes, humidifiers, preheaters, glass sealant, and even the raw materials of the cell components [19,21,22]. Another important but less understood source of silica is the feed water itself but exact purity requirements are still unclear. This uncertainty is further amplified by many research groups using hydrogen combustion to generate steam thereby avoiding direct water impurity carryover into the feed gas. Feed water quality is a critical factor for electrolysis plants, as it influences the design of the balance of plant (BoP) components, affects maintenance costs, and impacts the lifetime of the stacks, which are key determinants of final product costs.

DLR and Sunfire have systematically investigated the effect of silica impurities in state-of-the-art ESC with Ni/CGO fuel electrodes during steam and co-electrolysis in multiple German research projects to understand the degradation mechanism and develop mitigation strategies. In the present study, the influence of feed water quality on single cell degradation in co-electrolysis and the impacts of silica on performance and microstructure are examined.

## 2. Experimental

### 2.1. Electrochemical cell characterization

State-of-the-art electrolyte-supported cells with a size of 5 × 5 $cm^2$ and an active area of 4 × 4 $cm^2$ were supplied by Sunfire (Dresden, Germany). They consisted of a 90 µm thick 3 mol% $Y_2O_3$-doped $ZrO_2$ (3YSZ) electrolyte, 5 µm thick CGO interlayers on both the fuel and oxygen electrode side, a Ni/CGO fuel electrode with a functional layer and a more porous current collector layer with increased Ni content, and a $La_{0.6}Sr_{0.4}Co_{0.2}Fe_{0.8}O_{3-\delta}$ (LSCF)/CGO oxygen electrode with LSCF current collector layer.

Single cell testing was performed at DLR and the used setup has been illustrated and described in detail in earlier works [23,24]. The cells were mounted with the oxygen electrode pointing upwards and heated (3 K/min) to 860 °C for reduction and electrochemical testing. Proper sealing of all cells with Au frames was ensured by confirming the open circuit voltage (OCV) to be higher than 1.2 V in pure hydrogen and air. Carbon dioxide with a purity of 99.995 % and carbon monoxide with a purity of 99.0 % by Linde (München, Germany) were used in all experiments. Steam was provided via a controlled evaporator mixer (CEM) from Bronkhorst (Kamen, Germany) in which small water droplets are injected into a carrier gas stream at temperatures of 100–130 °C depending on the operating point. The fuel gas was then carried to the oven via heating pipes with polytetrafluoroethylene (PTFE) core with a maximum temperature of 130 °C. Subsequently, the fuel gas was brought to oven temperature by going through a ceramic pipe into the oven atmosphere.

Feed water was first purified via reverse osmosis, and in some experiments went through a ultrapure water supply installation including a mixed bed ion exchanger, a UV disinfection device, two particle filters (1 µm and 0.2 µm) and a conductivity measurement. If ultrapure water was used a maximum conductivity of 0.1 µS $cm^{-1}$ was ascertained for the duration of all experiments. Additionally, the mineral content of the feed water was analyzed with inductively coupled plasma mass spectrometry (ICP-MS) measurements, for which 100 µL nitric acid were added to the water samples for ionic stabilization.

The first experiment over ~1000 h was carried out with a fuel gas of 63.7 % $H_2O$, 31.3 % $CO_2$ and 5 % $H_2$ at a flow rate of 0.204 SLPM and with reverse osmosis (RO) feed water. An air flow rate of 0.5 SLPM and a current density of −0.92 A $cm^{-2}$ was used. At the beginning of this experiment, the humidifier had already been in operation in previous tests for several thousand hours.

Three additional experiments were performed at constant total fuel and air flow rates of 1 standard liter per minute (SLPM), respectively. The fuel gas composition was 50 % $H_2O$, 25 % $CO_2$, 20 % $N_2$ and 5 % $H_2$. Current densities of −0.25, −0.5 and − 1.0 A $cm^{-2}$ were applied for the different tests, respectively. The same humidifier as in the previous experiment was used and operated at the same temperature about 10 months after the first experiment with the only nominal change being the use of ultrapure water. Electrochemical impedance spectroscopy (EIS) was performed by means of an electrochemical workstation (Zahner PP-240 with Thales software) in a frequency range from 100 mHz to 100 kHz with 10 points per decade. The amplitude of the current stimulus was chosen to be 500 mA.

### 2.2. Post mortem analysis

Tested cell samples were embedded into a resin and microstructures of polished cross-section samples were investigated with a Zeiss ULTRA PLUS scanning electron microscope (SEM) (Carl Zeiss AG, Germany) in combination with a Bruker XFlash 5010 energy-dispersive X-ray spectroscopy (EDX) detector for elemental analysis.

Material phases were analyzed by X-ray diffraction (XRD) using a D8 ADVANCE (BRUKER AXS GmbH, Germany) device with a Cu Kα radiation source operating at 40 kV and 40 mA in Bragg-Brentano geometry with an increment step of 0.02° to identify the phases and determine their structural parameters.

## 3. Results and discussion

### 3.1. Single cell degradation in co-electrolysis with reverse osmosis feed water

As a first step, a 1000 h durability test was carried out using reverse osmosis water as feed for the humidifier. The cell was operated with a steam/carbon (S/C) ratio of 2 at −0.92 A $cm^{-2}$ corresponding to a reactant utilization of 60 %. The conditions were chosen to investigate the cell's behavior at relatively high current densities. Its voltage evolution is depicted in Fig. 1. The cell showed a degradation rate of 67.4 mV/kh (4.9 %/kh) over the course of the experiment. Fig. 1b+c show two impedance spectra, one at the beginning and one at the end of the durability test. Fig. 1b shows that the resistance increase of 77 mΩ $cm^2$ consisted mainly of an ohmic resistance increase of 70 mΩ $cm^2$ and a minor increase of the polarization resistance of 7 mΩ $cm^2$. This predominant degradation of the ohmic resistance is consistent with most other literature reports investigating the durability of state-of-the-art ESC in electrolysis operation and usually assumed to be governed by the loss of ionic conductivity in the YSZ electrolyte upon ageing [6–8], with possible contributions of the electrode/electrolyte interface [25]. However, the degradation rate observed in this experiment is significantly higher compared to previous literature studies with comparable cell configurations and testing conditions indicating the presence of one or more additional degradation phenomena [7]. The polarization resistance increase in Fig. 1 mainly occurred at frequencies of ~20 Hz attributed to a Ni/CGO surface process [23,26–28].

A post mortem analysis of the tested cell at the inlet showed major changes in the Ni/CGO fuel electrode microstructure as shown in the EDX mapping in Fig. 2 and in Table 1. A large amount of silica impurities was found in particular at the interface between the Ni/CGO functional layer and the CGO interlayer with molar percentages of up to 8.7 %. Smaller amounts of silica could also be found at the Ni current collector| Ni/CGO functional layer interface. Only traces of silica (<0.2 mol%) were found in the outlet suggesting the feed gas as its source. No indications of coking were observed.

Silica is well-known to dissolve in water as silicic acid $Si(OH)_4$

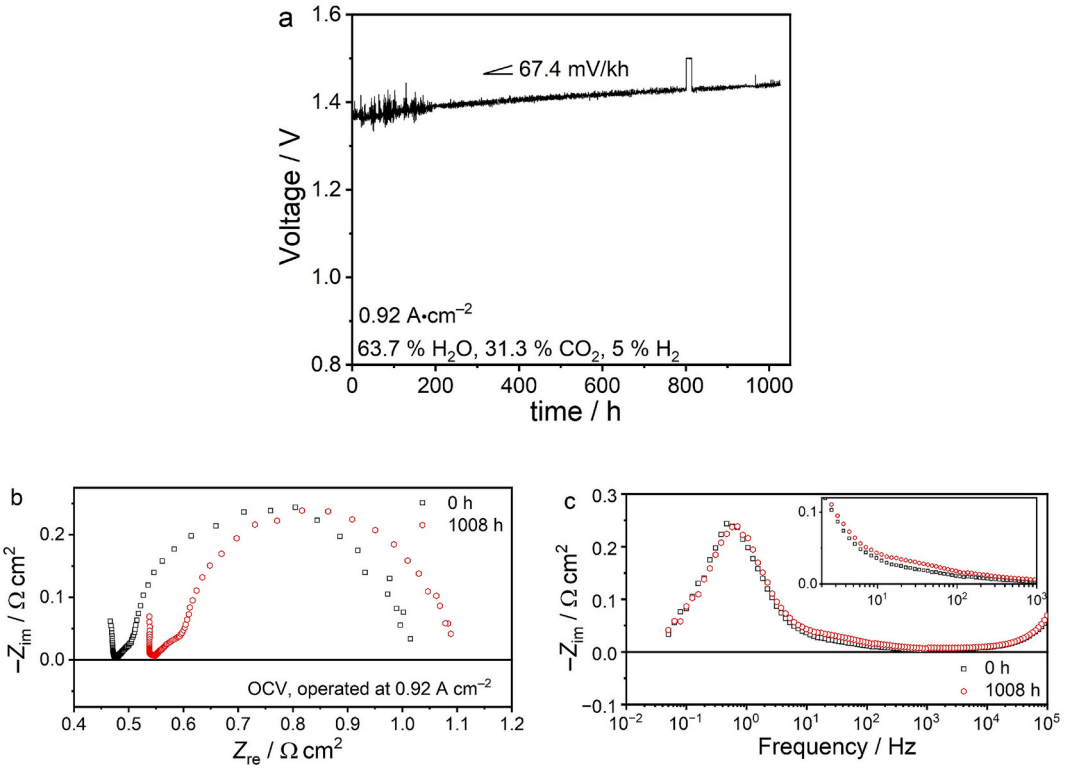


**Fig. 1.** (a) Voltage over time over 1000 h of an ESC at 860 °C, S/C = 2, −0.92 A $cm^{-2}$ and with a reactant conversion of 60 %. (a) Nyquist plot of the two impedance spectra before (0 h) and after (1008 h) the durability test (b) Imaginary impedance of the two spectra from (a).

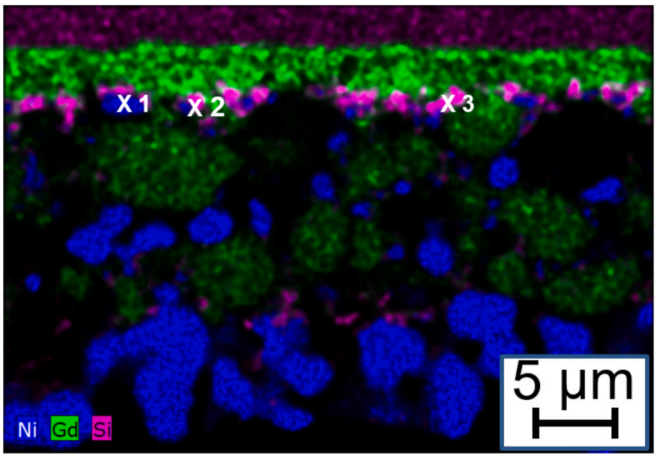


**Fig. 2.** EDX mapping of the inlet of the Ni/CGO fuel electrode of the ESC tested at −0.92 A $cm^{-2}$ for 1008 h.

**Table 1**
Molar percentages of different elements at three different spots in the fuel electrode as shown in Fig. 2, according to EDX analysis.

| Location | O | Al | Si | Ni | Ce | Gd |
|---|---|---|---|---|---|---|
| x 1 / % | 18.1 | 0.9 | 3.4 | 69.6 | 5.7 | 2.4 |
| x 2 / % | 42.4 | 1.1 | 8.7 | 24.8 | 16.8 | 6.3 |
| x 3 / % | 48.2 | 0.9 | 8.1 | 11.4 | 23.8 | 7.6 |

[29,30] which is a weak acid according to

$$SiO_2(s) + 2\,H_2O \rightarrow Si(OH)_4\,(g) \quad (1)$$

and can migrate to the steam phase via carryover [21]. According to (1), it is likely that solid silica ($SiO_2$) in an amorphous state will deposit in the fuel electrode regions with the lowest steam content, that is, the electrode/electrolyte interface. The deposition of considerable amounts of silica at the interface could physically block and deactivate the electrochemically active sites on the fuel electrode, leading to an increase in charge transfer resistance. Additionally, this deposition could effectively extend the electrolyte thickness, contributing to the observed rise in ohmic resistance.

XRD analysis of the fuel electrode inlet of the cell from top view showed peaks corresponding to the Ni and CGO10 surface, along with an additional peak at 31° with a shoulder peak at slightly higher angles (see Fig. 3). This additional peak is most likely associated with the primary peak of the cerium silicate phase $Ce_{4.67}(SiO_4)_3O$. No $SiO_2$-related peaks

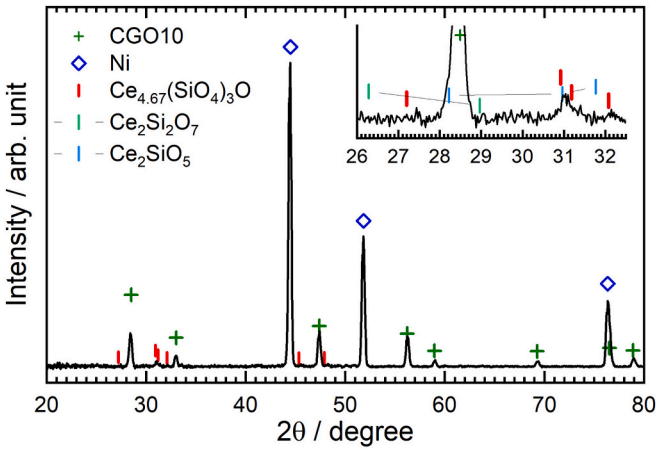


**Fig. 3.** XRD pattern of the top view fuel electrode inlet of the cell operated for 1008 h with reverse osmosis water. ($Ce_{4.67}(SiO_4)_3O$ (04–007-9162), $Ce_2(Si_2O_7)$ (04–019-7677), $Ce_2SiO_5$ (00–048-0054)).

were identified suggesting a reaction between ceria and silica. The chemical reaction of silica and ceria in reducing atmospheres with the formation of different silicate phases such as $Ce_{4.67}(SiO_4)_3O$, $Ce_2Si_2O_7$ and $Ce_2SiO_5$ has been observed previously. [31,32] $Ce_{4.67}(SiO_4)_3O$ was reported to be the most stable among them, forming at temperatures as low as 1000 °C [31]. The application of a cathodic bias to the Ni/CGO fuel electrode in the present study could have further promoted the formation of cerium silicates. The formation of cerium silicates and the corresponding change of the CGO transport properties and surface exchange rate could be a plausible mechanism for the increase in ohmic and polarization resistance of the cell reported in Fig. 1.

Silicon carbonate $SiCO_4$ also exists, but high pressures of 18–26 GPa and temperatures 600–980 K are required for its formation from $SiO_2$ and $CO_2$, making it thermodynamic unstable under the conditions of this study [33].

A recent study identified quartz glass insulation in preheaters as a prominent source of silica since it could corroded by steam according to eq. 1, particularly at higher temperatures >300 °C [21]. However, in the present experiment the fuel gas was preheated outside the oven in the humidifier and then carried through heating pipes with a maximum temperature of 130 °C. Subsequently, the fuel gas was heated to oven temperature via an alumina pipe already in the oven atmosphere. Thus, the reverse osmosis feed water was identified as possible origin of the silica impurities and analyzed by means of ICP-MS at the time of the experiment. Table 2 gives an overview of different trace impurities in the reverse osmosis water, and shows indeed the presence of ~43 μg $L^{-1}$ (43 ppb) silica in the water. Furthermore, significant concentrations of Cu and Zn were detected, possibly originating from brass pipes downstream of the central reverse osmosis water system. However, no depositions of Cu/Zn were detected in the fuel electrode by means of EDX.

### 3.2. Single cell degradation in co-electrolysis with ultrapure water

As a next step, the durability of ESC in co-electrolysis was tested after the installation of a ultrapure water supply. The conductivity of the feed water was continuously monitored to be below 0.1 μS $cm^{-1}$. However, since silica/silicic acid (see eq. 1) are not fully dissociated in water they do not increase the conductivity of purified water very strongly once a breakthrough of the ion exchanger occurs. Therefore, feed water samples were analyzed by ICP-MS directly after the ion exchanger as well (see Table 2). Results of the water analysis in Table 2 showed that the ultrapure water had a significantly lower silica content than the reverse osmosis water below the detection limit. Thus, the use of mixed bed ion exchangers is an effective means to remove silica from the feed water, as well as all other measured elements (all below DL).

A mixed bed ion exchanger consists of both a strong acid cation resin, which removes positively charged ions, as well as a strong base anion (SBA) resin, which captures negatively charged species, including sulfate, chloride, and silica. Since silica is present in water as either monosilicic acid ($Si(OH)_4$) or silicate ions ($SiO_4^{2-}$, $HSiO_3^-$) depending on the pH, the removal process involves anion exchange, where negatively charged silicate species ($HSiO_3^-$, $SiO_4^{2-}$) are effectively captured by the SBA resin [34]. In this process, hydroxide ($OH^-$) ions from the resin are exchanged for negatively charged silicate species, leading to their removal from the water. The exchange process increases the local pH, further driving the increasing charging of dissolved silica species, facilitating their removal according to the following equilibria.

$$Si(OH)_4 + OH^- \rightarrow HSiO_3^- + H_2O \quad (2)$$

$$HSiO_3^- + OH^- \rightarrow SiO_3^{2-} + H_2O \quad (3)$$

This approach ensures highly efficient deionization and silica removal, achieving a purity level beyond what reverse osmosis can provide. While RO membranes can effectively reject colloidal and polymerized silica, they are less effective against dissolved reactive silica, which can pass through the membrane due to its weakly ionized nature. High silica concentrations in RO systems can even increase the risk of membrane fouling and degradation over time [34]. By using mixed bed ion exchange as a final polishing step, silica levels in ultrapure water are reduced below the detection limit, ensuring high water quality.

The analysis of the condensed water behind the humidifier and heating pipes also showed the absence of silica species indicating that impurities in the experiment shown in the previous section likely did not originate from these auxiliary components. However, trace amounts of Mn, Cu, Co and Ni were detected that were most likely leached from either the humidifier, the steel fittings or the heating pipes. The ultrapure water samples shown in Table 2 were taken shortly after the end of the electrochemical experiments shown in Fig. 4 and represent the best estimate for the water quality at the time. Additional water analyses in recent years have shown that impurity concentrations fluctuate over time to a certain extent which could be related to the lifetime of the mixed bed ion exchanger in the ultrapure water installation. However, the maximum Si concentration in the ultrapure water ever measured was only 4 μg $L^{-1}$.

Degradation tests of three ESCs at −0.25, −0.5 and − 1 A $cm^{-2}$ in co-electrolysis over ~1500 h using the ultrapure water are depicted in Fig. 4a. The cells operated at −0.25 and − 0.5 A $cm^{-2}$ showed an activation in the first ~450 h causing a decrease of the ohmic resistance (see Fig. 4b, Fig. 5). This activation behavior was related to the softening of the Au contacting meshes on the oxygen electrode causing an improvement of contact and thus, ohmic resistance over time (Fig. 5). For this reason, only the degradation rates between ~450 h and the end of the experiment were calculated for all cells. The relative voltage degradation rates (see Table 3) of 0.47 %/kh (−0.5 A $cm^{-2}$), 0.67 %/kh (−0.25 A $cm^{-2}$) and 0.97 %/kh (−1.0 A $cm^{-2}$) are close to the 0.5 %/kh targeted by the European Clean Hydrogen Joint Undertaking by 2030 [5], and can be expected to further decrease upon operation for longer time periods [7].

The three cells were operated at conditions slightly different from the cell operated with reverse osmosis water, however, they showed voltage degradation rates >5 times lower than the 4.9 %/kh of the cell operated with reverse osmosis water suggesting a pronounced beneficial influence of the feed water quality on the cells' long-term stability.

For a direct comparison of the degradation of the cells operated at different current densities, impedance spectra were recorded for all cells at the same operating conditions at OCV. After the initial activation period at ~450 h, all three cells showed similar ohmic resistances of 0.465–0.48 Ω $cm^2$ and polarization resistances of 0.155–0.175 Ω $cm^2$ demonstrating the reproducibility of the cells. In the following, the area-specific resistance (ASR) degradation rates of the three cells was between 10.4 and 14.8 mΩ $cm^2$/kh, almost entirely due to an increase of the ohmic resistance for all cells. Recently, we showed that sulfur impurities in the same $CO_2$ feed gas as used in the present study can lead to severe Ni surface poisoning and degradation [17]. While this was especially pronounced during $CO_2$ electrolysis, smaller performance drops were also observed in $H_2/H_2O/CO_2/CO$ mixtures. In the present

**Table 2**
Trace impurity concentrations in the different water sources determined by ICP-MS. Detection limit (DL) was 1 μg $L^{-1}$ for Si, 0.1 μg $L^{-1}$ for the other elements. Li, B, Al, P, S, K, Ca, Cr, Fe, Ba, Tl and Pb were also analyzed and no signal above the DL was detected.

| Species | Reverse osmosis water / μg $l^{-1}$ | Ultrapure water source / μg $l^{-1}$ | Ultrapure water after humidifier & heating pipe / μg $l^{-1}$ |
|---|---|---|---|
| Si | 43.3 | <DL | <DL |
| Mn | 0.2 | <DL | 8.2 |
| Co | <DL | <DL | 0.1 |
| Ni | 0.2 | <DL | 8.4 |
| Cu | 47.7 | <DL | 0.5 |
| Zn | 63.6 | <DL | <DL |

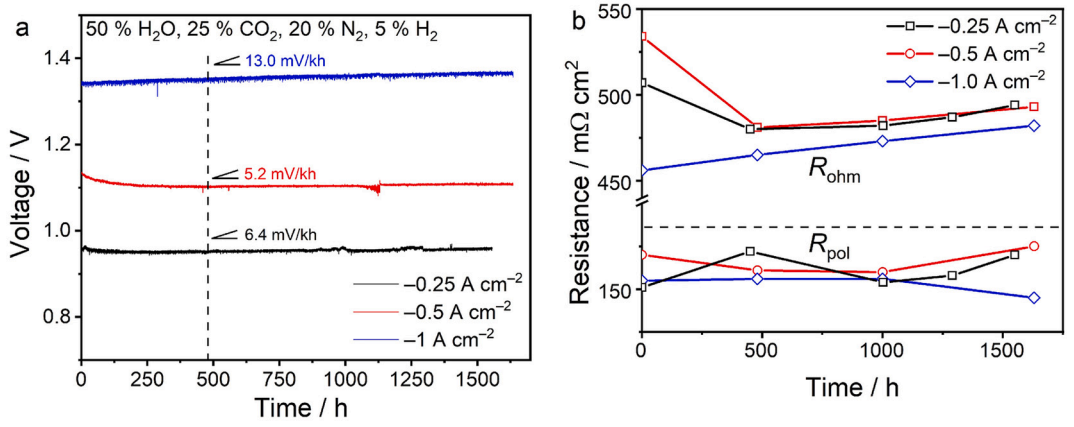


**Fig. 4.** (a) Voltage over time over ~1600 h of three ESC at 860 °C, S/C = 2, −0.25, −0.5 and − 1.0 A cm$^{-2}$. (b) Polarization and ohmic resistance of the three cells over time extracted from electrochemical impedance spectra.

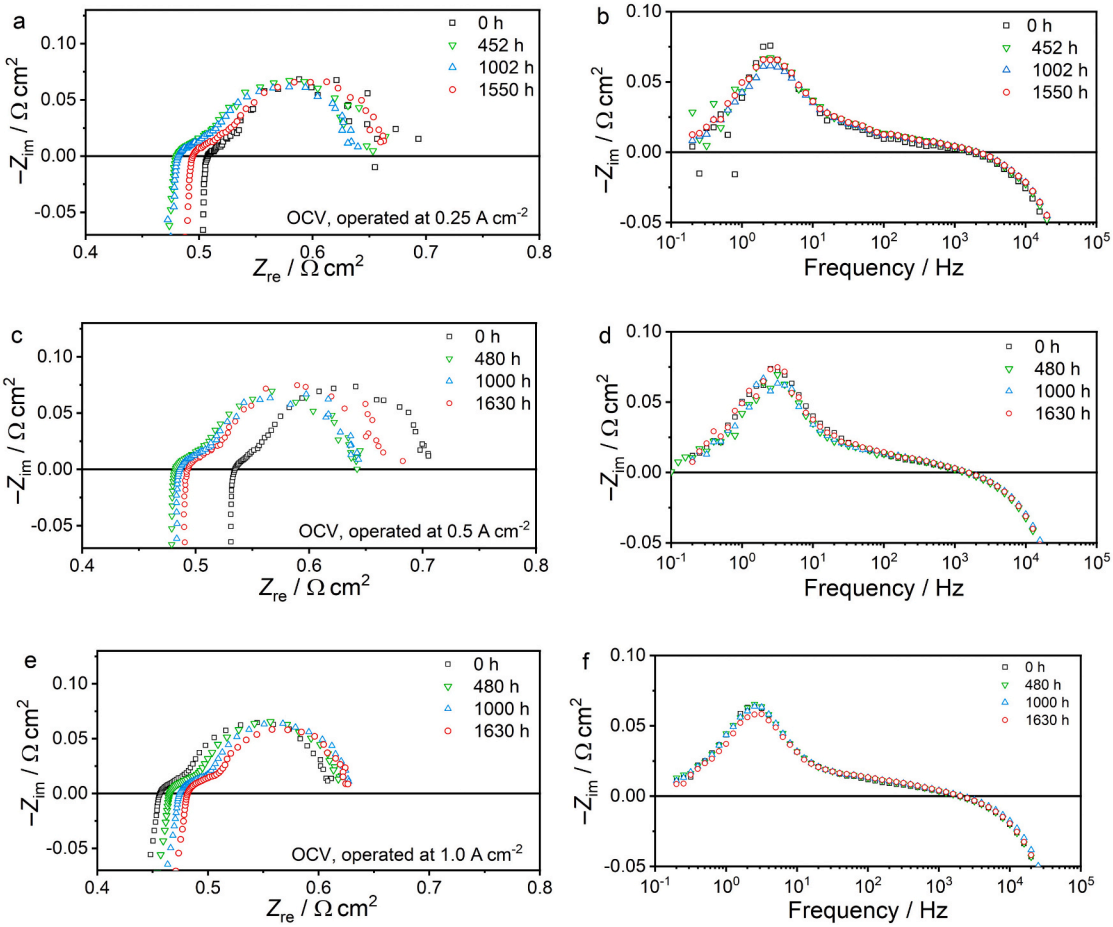


**Fig. 5.** Nyquist and imaginary impedance plots at different times during the durability test shown in Fig. 4 in co-electrolysis at (a + b) -0.25 A cm$^{-2}$, (c + d) -0.5 A cm$^{-2}$, and (e + f) -1.0 A cm$^{-2}$.

study, the Ni/CGO surface processes remained unaffected over the course of the experiments indicating the absence of sulfur-induced degradation. The reason could possibly be the larger $H_2O/CO_2$ ratio leading to an abundance of atomic hydrogen on the Ni surface and the enhanced removal of sulfur from the surface as already suggested previously [17].

The main change of the polarization resistances occurred at frequencies around 1 Hz associated with the gas conversion (Fig. 5) [35]. Since the gas streams of the three cells in the testing setup were connected, it is likely that changes in the gas conversion resistance rather reflected small changes in the pressure distribution between the different inlet streams than physico-chemical phenomena in the cell. As the change of the imaginary impedance over time at the other frequency regions was negligible for all cells, the ohmic resistance changes were used for calculation of the degradation rates in Table 3.

Although the cell operated at −1.0 A cm$^{-2}$ showed the highest degradation rate, no clear trend with regards to the effect of current density could be derived. However, longer operating times will be

**Table 3**
Overview of the different durability experiments and the corresponding degradation rates. Reverse osmosis water was used during the −0.92 A $cm^{-2}$ test, ultrapure water was used during the other three tests.

| Current density / A $cm^{-2}$ | Beginning / h | End / h | ASR degradation rate / mΩ $cm^2$/kh | Voltage degradation / mV/kh |
|---|---|---|---|---|
| −0.92 | 0 | 1008 | 76.4 (7.5 %/kh) | 67.4 (4.9 %/kh) |
| −0.25 | 450 | 1550 | 12.7 (2.0 %/kh) | 6.4 (0.67 %/kh) |
| −0.5 | 480 | 1630 | 10.4 (1.6 %/kh) | 5.2 (0.47 %/kh) |
| −1 | 480 | 1630 | 14.8 (2.4 %/kh) | 13 (0.97 %/kh) |

necessary to allow identification of such a hypothetical trend since the observed degradation rates of this state-of-the-art technology are very low.

The increase of the ohmic resistance for all three cells is often assumed to be governed by the degradation of the electrolyte over time since a gradual decrease of the ionic conductivity of YSZ over time is well-known to increase the cells' ohmic losses [36–38]. Different underlying mechanisms have been suggested such as segregation of the dopant cations to the grain boundaries, precipitation of the tetragonal phase, segregation of impurities at the grain boundaries, and disorder–order transformations in the crystal structure of the doped zirconia. Besides the degradation of the electrolyte, other mechanisms could contribute to the ohmic resistance increase such as the growth of the strontium zirconate phase and the interdiffusion zone at the LSCF|CGO|YSZ interface [25]. However, the detailed post mortem analysis of these interfaces/interphases is outside the scope of the present work.

In general, the observed degradation rates of 10.4–14.8 mΩ $cm^2$/kh are higher than the ASR degradation rate of 8 mΩ $cm^2$/kh over 23,000 h reported for a single cell with a similar architecture in steam electrolysis [7]. In that long-term study, decreasing degradation rates over time were observed which is most likely the reason for the increased degradation rates in the present study. Durability tests of Sunfire stacks at DLR and Sunfire revealed degradation rates of 12–18 mΩ $cm^2$/kh in steam electrolysis [6,8,39]. In general, the observed degradation rates in the present study are similar to, or slightly lower than these reported literature values, most likely due to the occurrence of stack-specific degradation mechanisms that are not observed at cell level, such as progressing chromia scale growth in the interconnect, Cr poisoning of the oxygen electrode, and leaching of contaminants from the glass sealant in wet atmospheres. Based on these values, it is considered likely that co-electrolysis operation of the employed ESC technology in the absence of severe impurity-induced degradation does not lead to higher degradation rates than under steam electrolysis. This finding was also previously confirmed in durability tests of ESC-based stacks by Fraunhofer IKTS that showed similar degradation rates (0.5 %/kh, 17 mΩ $cm^2$/kh) in steam and co-electrolysis [9].

In our previous degradation study of state-of-the-art cathode-supported cells in steam electrolysis, we observed ohmic resistance degradation rates between 21 mΩ $cm^2$/kh (at −0.5 A $cm^{-2}$) and 39 mΩ $cm^2$/kh (at −1.0 A $cm^{-2}$) under similar conditions at 850 °C demonstrating the high stability of the ESC technology in the present study [40].

EDX mappings of the Ni/CGO fuel electrode inlet of the cell tested at −1.0 A $cm^{-2}$ are depicted in Fig. 6. Some spots in the Ni-rich current collector layer (x 1 and × 2) showed only locally confined accumulation of silica species of up to 6.5 mol% (see Table 4). However, in general no enrichment of silica species was observed at the electrode/electrolyte interface indicating that the input of silica via the feed water was drastically reduced. Neither Mn, Co, Cu nor Zn were observed in the fuel electrode by means of EDX. Similar results were obtained for the cells operated at lower current densities.

In addition, no Ni migration was observed at the electrode/electrolyte interface demonstrating that Ni/CGO fuel electrodes are resistant

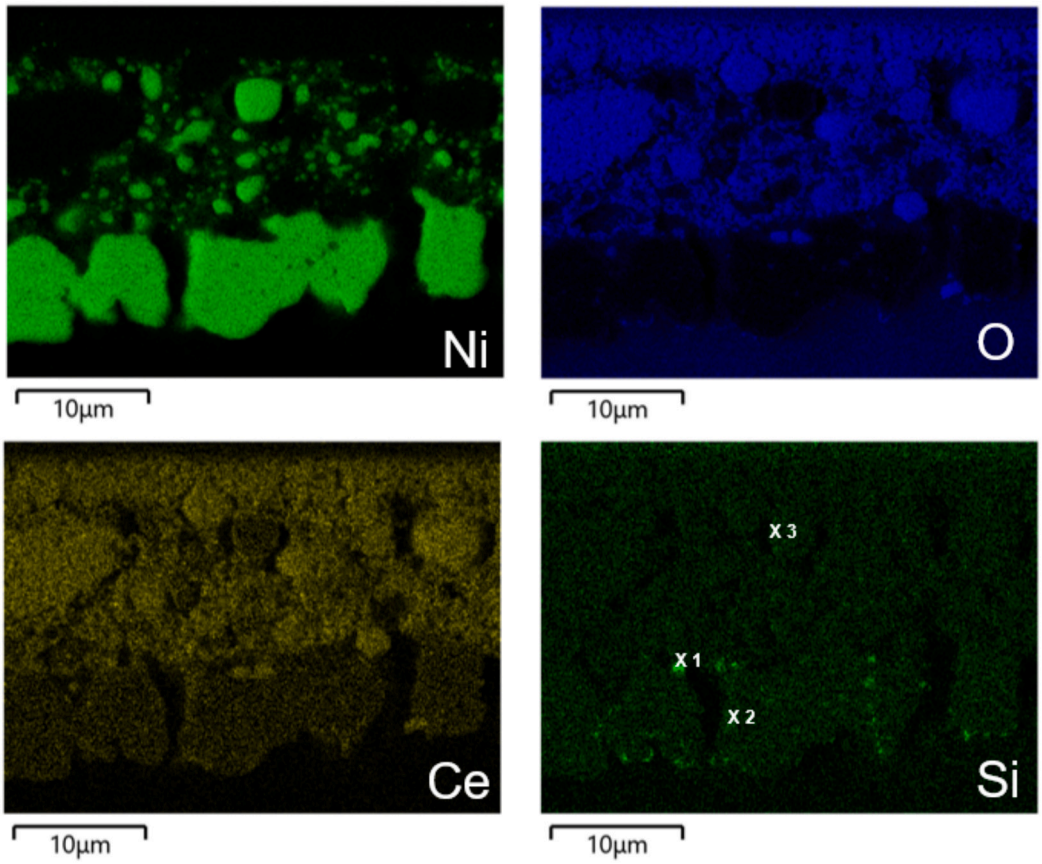


**Fig. 6.** EDX mappings of the inlet of the Ni/CGO fuel electrode of the ESC tested at −1.0 A $cm^{-2}$ for 1500 h.

**Table 4**
Molar percentages of different elements at three different spots in the fuel electrode as shown in Fig. 6, according to EDX analysis.

| Location | O / mol% | Si/ mol% | Ni/ mol% | Ce/ mol% | Gd/ mol % |
|---|---|---|---|---|---|
| x 1 | 38.3 | 6.5 | 45.6 | 8.0 | 1.6 |
| x 2 | 7.4 | 1.0 | 90.3 | 1.3 | – |
| x 3 | 14.8 | – | 69.6 | 13.8 | 1.4 |

against this degradation mechanism in the typical ESC co-electrolysis operating conditions employed in the present study. However, it is still unclear if Ni migration could occur at current densities >1 A $cm^{-2}$ in pure steam electrolysis where Ni migration was observed to be most pronounced in fuel electrode supported cells [40].

### 3.3. Post mortem analysis of degraded full stack

Furthermore, the post mortem analysis of a 30-cell stack by Sunfire AG was carried out after its electrochemical investigation. The ESCs were composed of the same materials as described in the previous subsection and had an active area of 128 $cm^2$. For increased mechanical stability, the stack contained intermediate plate after each 10 repeat units (RUs). The interconnector plates consisted of Crofer22APU ferritic steel. The stack used an open-air manifold and a co-flow design. RUs are numbered from top to bottom. More details are given in previous studies of the same stack type [6,41,42].

The electrochemical tests, conducted as part of a separate study at Forschungszentrum Jülich, provided the operational context but are beyond the scope of this work. The electrochemical results are described in Ref. [43] In short, the stack was in a hot state for 3500 h in total, and operated for ~1300 h in steam electrolysis at the commonly used nominal operating conditions (see also Ref. [6,41,42]), where it showed an unusually large degradation rate of up to 200–300 mΩ $cm^2$/kh.

Thus, the degradation was significantly higher than the values observed for single cells in co-electrolysis with ultrapure water as shown earlier, and also higher than the 0.5–0.8 %/kh or 12–18 mΩ $cm^2$/kh previously reported for long-term steam electrolysis tests of 30-cell stacks from Sunfire [6,39,44]. For this reason, the occurrence of at least one accelerated degradation mechanism was expected. Compared to the voltage increase in electrolysis operation, the stack voltage was observed to be relatively stable in fuel cell operation. For this reason, it is concluded that the degradation was mainly due to the stack operation in steam electrolysis mode.

The present paper aims to complement such data by providing a detailed post mortem analysis to elucidate the structural and material changes that occur during operation.

A representative photographed image of the fuel electrode side of a full-size cell taken from the middle of the long-term operated ESC stack showed a change of color from dark grey at the inlet of cell to a lighter grey at the outlet of the cell (Fig. 7). SEM images (Fig. 8) and EDX mappings (Fig. 9) were recorded at different locations along the channel in the transition zone (see 1–4 in Fig. 8), and the macroscopic color change could be correlated with significant alterations in the fuel electrode microstructure, in particular a decreasing silica content along the channel.

The CGO adhesion layer at the inlet of the cell at position 1 (Fig. 8a) but also to a smaller extent at position 2 (Fig. 8b) showed a high degree of densification. The EDX mapping in Fig. 9a displayed a large amount of silica in this region. No clear difference between the CGO particles and the deposited silica could be observed in the microstructure in Fig. 8a, indicating the possibility of the formation of a new phase via reaction of CGO and silica. Similar to the observations in Fig. 2, silica accumulated mainly at the electrolyte|fuel electrode interface where steam partial pressures were lowest.

A comparison of the fuel electrode microstructure and composition between position 2 and position 3 showed a considerable decrease in silica content at position 3, suggesting the macroscopic color change in Fig. 8 to be due to the extent of silica deposition in the fuel electrode. Only traces of silica could be found in position 4, indicating that the impurities were mainly carried into the stack with the feed gas. Ni in the functional layer of this silica-free location looks has coarsened compared to a reduced electrode of the same cell type [45], but has not migrated away from the electrode/electrolyte interface. The progressive fuel electrode color change along the channel suggests that the silica impurities were introduced by the feed gas. Most likely, the primary source of silica contamination was the quartz glass insulation in the fuel gas preheater at Forschungszentrum Jülich, which has been shown to release above 400 µg $L^{-1}$ of silicon contaminants into the fuel gas phase [21]. The feed water of the stack test also contained non-negligible amounts of silica and could have contributed to the contamination as well. However, no detailed water analysis is available for this test.

Nickel surfaces are well-known to be susceptible towards sulfur poisoning and coking which leads to large performance drops in Ni/cermet electrodes upon sulfur and carbon accumulation on the nickel surface. However, nickel has not been observed to be particularly vulnerable towards silica poisoning. Silica-supported nickel catalysts are even frequently employed in heterogeneous catalysis applications such as high-temperature methane pyrolysis [46]. Silica-induced degradation has previously been reported to occur in Ni/YSZ fuel electrode during steam electrolysis. However, silica was observed to segregate at the Ni/YSZ interface rather than poisoning the nickel surface [19,47]. By contrast, metal oxides were reported to be vulnerable towards silica poisoning with silica impurities known to negatively affect the grain

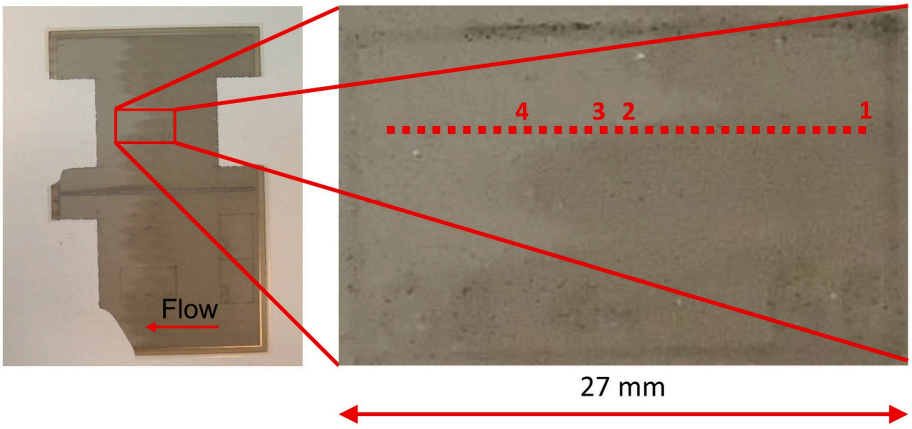


**Fig. 7.** Photograph of the fuel electrode side of a full cell taken from a stack operated long-term in co-electrolysis. Numbers from 1 to 4 denote the locations for further SEM/EDX analysis in Figs. 8+9.

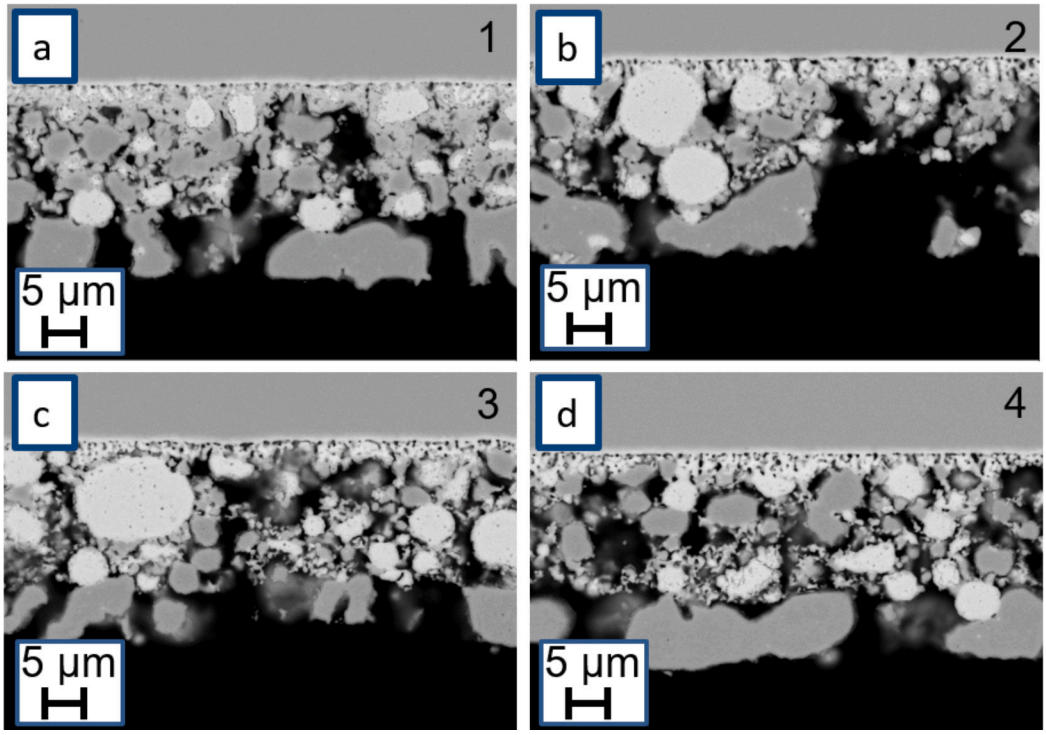


**Fig. 8.** SEM images of the Ni/CGO fuel electrode at different locations along the channel as indicated in Fig. 7.

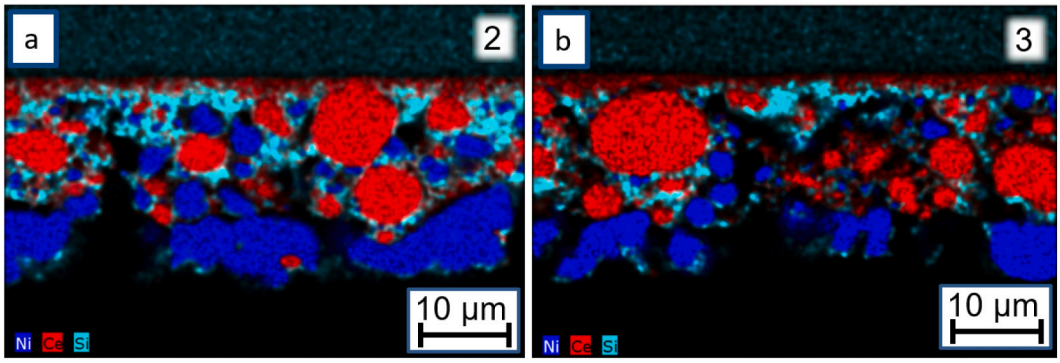


**Fig. 9.** EDX mappings of the Ni/CGO fuel electrode at locations (a) 2 and (b) 3 along the channel as indicated in Fig. 8. Note that both EDX mappings were slightly shifted to the right compared to the SEM images in Fig. 8b+c.

boundary ionic conductivity and metal oxide surface oxygen exchange rates [48]. When large amounts of silica are present impenetrable Si-rich glassy layers can be formed resulting in surface blockage. Even at lower Si surface concentrations, the acidic silica not only blocks the metal oxide surface, but also induces an electron depletion region which hampers the charge transfer reaction [48,49]. The large-scale accumulation of silica including the clogging of pores in the vicinity of the CGO interlayer in the present study and the formation of cerium silicate seem to be phenomena not observed for Ni/YSZ electrodes, indicating that CGO could act as a scavenger for silica.

The formation of cerium silicates in Ni/CGO electrodes highlights a broader issue of silica transport and deposition in high-temperature steam-based systems, particularly in steam turbines [50]. In both solid oxide cells and steam turbines, volatile $Si(OH)_4$ species present in the steam phase can be transported through the system and subsequently deposit on critical surfaces, leading to performance degradation. Similar to silicate formation in Ni/CGO fuel electrodes, silica scaling in steam turbines occurs when silica carried over with steam precipitates onto turbine blades and steam pathways, forming deposits that reduce heat transfer efficiency and increase maintenance requirements. In both cases, deposition is influenced by temperature, pressure steam composition, and material reactivity, with high-temperature regions being particularly vulnerable. These parallels suggest that mitigation strategies used in steam turbines, such as strict water purity control and advanced filtration methods, could provide insights for reducing silica-related degradation during SOEL.

## 4. Summary and conclusions

This study provides the first detailed documentation of the negative impact of silicate formation in Ni/CGO fuel electrodes in high-temperature SOEL. It was demonstrated that Ni/CGO fuel electrodes can undergo severe degradation due to the large-scale deposition of silica impurities at the electrolyte|electrode interface and the formation of the cerium silicate phase $Ce_{4.67}(SiO_4)_3O$. In contrast to Ni/YSZ fuel electrodes, no indications of $SiO_2$ formation was detected. The feed water was identified as a major source of silica impurities, emphasizing the need for water with silica concentrations below 1 ppb to achieve low

single cell degradation rates of 10.4 mΩ $cm^2$/kh in co-electrolysis. Degradation rates increased by a factor of 3–5 upon the use of reverse osmosis water with a silica content of >40 ppb. The relationship between degradation and water purity was supported by water analyses at the time of various durability tests, with notable reductions in degradation following the introduction of an ultrapure water supply. After 1500 h of single cell co-electrolysis operation using ultrapure feed water, no significant accumulation of silica impurities was observed in the Ni/CGO fuel electrode, suggesting the successful mitigation of this degradation mechanism within the test period.

However, the potential for silica contamination from other sources, such as BoP components, remains a concern for long-term operation. This underscores the importance of suitable BoP component design to avoid the carryover of silica from electric heaters, heat exchangers and hotbox steels into the fuel gas. Future research should focus on controlled experiments with intentional silica dosing and real-time concentration monitoring to further elucidate the mechanisms of cerium silicate formation. Furthermore, strategies to enhance SOEC tolerance towards silica deposition, such as developing alternative fuel electrode materials, are neede3d to avoid accelerated degradation upon breakthrough of the water purification units.

## CRediT authorship contribution statement

**Matthias Riegraf:** Writing – original draft, Methodology, Investigation, Formal analysis, Data curation, Conceptualization. **Alexander Surrey:** Writing – review & editing, Investigation, Funding acquisition, Formal analysis, Data curation. **Noriko Sata:** Writing – review & editing, Investigation, Formal analysis, Data curation. **Rémi Costa:** Writing – review & editing, Supervision, Resources, Project administration, Methodology, Investigation, Funding acquisition, Conceptualization.

## Declaration of competing interest

The authors declare the following financial interests/personal relationships which may be considered as potential competing interests: Matthias Riegraf reports financial support was provided by The German Ministry of Education and Research. If there are other authors, they declare that they have no known competing financial interests or personal relationships that could have appeared to influence the work reported in this paper.

## Acknowledgements

The German Ministry of Education and Research (BMBF) is acknowledged for funding in the framework of the “Kopernikus Project P2X” and the “Kopernikus P2X-II” project under grant numbers 03SFK2E0 and 03SFK2E0-2. We would like to thank Diana Maria Amaya-Duenas for help with cell testing. Chen-Yu Tsai and Christian Geipel from Sunfire AG are acknowledged for the supply of cells and helpful discussions.

## Appendix A. Supplementary data

Supplementary data to this article can be found online at https://doi.org/10.1016/j.cej.2025.164654.

## Data availability

No data was used for the research described in the article.

## References

[1] Z.J. Schiffer, K. Manthiram, Electrification and Decarbonization of the chemical industry, Joule 1 (1) (2017) 10–14, https://doi.org/10.1016/j.joule.2017.07.008.
[2] M. Riegraf, R. Costa, K.A. Friedrich, Electrolyzer – solid oxide electrolyzer | overview, in: J. Garche (Ed.), Encyclopedia of Electrochemical Power Sources, Second Edition, Elsevier, 2025, pp. 109–122, https://doi.org/10.1016/B978-0-323-96022-9.00194-8.
[3] O. Posdziech, K. Schwarze, J. Brabandt, Efficient hydrogen production for industry and electricity storage via high-temperature electrolysis, Int. J. Hydrog. Energy 44 (35) (2019) 19089–19101, https://doi.org/10.1016/j.ijhydene.2018.05.169.
[4] H. Böhm, M. Lehner, T. Kienberger, Techno-economic assessment of thermally integrated co-electrolysis and methanation for industrial closed carbon cycles, Front. Sustain. 2 (2021) 726332.
[5] Clean Hydrogen Joint Undertaking, Strategic Research and Innovation, Agenda 2021–2027. https://www.clean-hydrogen.europa.eu/system/files/2022-02/Clean%20Hydrogen%20JU%20SRIA%20-%20approved%20by%20GB%20-%20clean%20for%20publication%20%28ID%2013246486%29.pdf, 2024 accessed on January 8.
[6] M. Lang, S. Raab, M.S. Lemcke, C. Bohn, M. Pysik, Long-term behavior of a solid oxide Electrolyzer (SOEC) stack▲, Fuel Cells 20 (6) (2020) 690–700.
[7] J. Schefold, A. Brisse, H. Poepke, 23,000 h steam electrolysis with an electrolyte supported solid oxide cell, Int. J. Hydrog. Energy 42 (19) (2017) 13415–13426, https://doi.org/10.1016/j.ijhydene.2017.01.072.
[8] M. Riedel, M.P. Heddrich, K.A. Friedrich, Investigation of the long-term stability of solid oxide electrolysis stacks under pressurized conditions in exothermic steam and co-electrolysis mode, Fuel Cells 20 (5) (2020) 592–607.
[9] S. Megel, C. Dosch, S. Rothe, C. Folgner, N. Trofimenko, A. Rost, M. Kusnezoff, E. Reichelt, M. Jahn, A. Michaelis, et al., Co-electrolysis with CFY-stacks, ECS Trans. 78 (1) (2017) 3089, https://doi.org/10.1149/07801.3089ecst.
[10] G. Rinaldi, S. Diethelm, E. Oveisi, P. Burdet, J. Van Herle, D. Montinaro, Q. Fu, A. Brisse, Post-test analysis on a solid oxide cell stack operated for 10,700 hours in steam electrolysis mode, Fuel Cells 17 (4) (2017) 541–549.
[11] M. Riegraf, P. Szabo, M. Lang, R. Costa, S. Rothe, S. Megel, M. Kusnezoff, Electrochemical analysis of an electrolyte-supported solid oxide cell-based MK35x stack during long-term electrolysis operation, J. Electrochem. Soc. 171 (2024) 054504, https://doi.org/10.1149/1945-7111/ad417f.
[12] M. Riegraf, P. Szabo, M. Lang, R. Costa, S. Rothe, S. Megel, M. Kusnezoff, Reversible long-term operation of a MK35x electrolyte-supported solid oxide cell-based stack, J. Electrochem. Soc. 171 (10) (2024) 104505, https://doi.org/10.1149/1945-7111/ad8036.
[13] D. Schäfer, Q. Fang, L. Blum, D. Stolten, Syngas production performance and degradation analysis of a solid oxide electrolyzer stack, J. Power Sources 433 (2019) 126666, https://doi.org/10.1016/j.jpowsour.2019.05.072.
[14] A. Hauch, R. Küngas, P. Blennow, A.B. Hansen, J.B. Hansen, B.V. Mathiesen, M. B. Mogensen, Recent advances in solid oxide cell technology for electrolysis, Science 370 (6513) (2020) eaba6118, https://doi.org/10.1126/science.aba6118 (acccessed 2022/03/03).
[15] A. Hauch, M.L. Traulsen, R. Küngas, T.L. Skafte, CO2 electrolysis–gas impurities and electrode overpotential causing detrimental carbon deposition, J. Power Sources 506 (2021) 230108.
[16] T.L. Skafte, P. Blennow, J. Hjelm, C. Graves, Carbon deposition and sulfur poisoning during CO2 electrolysis in nickel-based solid oxide cell electrodes, J. Power Sources 373 (2018) 54–60.
[17] M. Riegraf, K. Develos-Bagarinao, I. Biswas, R. Costa, The influence of sulfur impurities in industrial COx gases on solid oxide electrolysis cell (SOEC) degradation, J. Power Sources 559 (2023) 232669, https://doi.org/10.1016/j.jpowsour.2023.232669.
[18] T.L. Skafte, Z. Guan, M.L. Machala, C.B. Gopal, M. Monti, L. Martinez, E. Stamate, S. Sanna, J.A. Garrido Torres, E.J. Crumlin, et al., Selective high-temperature CO2 electrolysis enabled by oxidized carbon intermediates, Nat. Energy 4 (10) (2019) 846–855, https://doi.org/10.1038/s41560-019-0457-4.
[19] A. Hauch, S.r.H.j. Jensen, J.r.B. Bilde-Sørensen, M. Mogensen, Silica segregation in the Ni/YSZ electrode, J. Electrochem. Soc. 154 (7) (2007), https://doi.org/10.1149/1.2733861. A619.
[20] M.B. Mogensen, A. Hauch, X. Sun, M. Chen, Y. Tao, S.D. Ebbesen, K.V. Hansen, P. V. Hendriksen, Relation between Ni particle shape change and Ni migration in Ni–YSZ electrodes – a hypothesis, Fuel Cells 17 (4) (2017) 434–441, https://doi.org/10.1002/fuce.201600222.
[21] D. Schäfer, L. Queda, V. Nischwitz, Q. Fang, L. Blum, Origin of steam contaminants and degradation of solid-oxide electrolysis stacks, Processes 10 (3) (2022) 598.
[22] M. Lankin, Y. Du, C. Finnerty, A review of the implications of silica in solid oxide fuel cells, J. Fuel Cell Sci. Technol. 8 (5) (2011) 054001–054007, https://doi.org/10.1115/1.4003980.
[23] M. Riegraf, V. Yurkiv, R. Costa, G. Schiller, K.A. Friedrich, Evaluation of the effect of sulfur on the performance of nickel/gadolinium-doped ceria based solid oxide fuel cell anodes, ChemSusChem 10 (3) (2017) 587–599, https://doi.org/10.1002/cssc.201601320.
[24] M. Riegraf, M.P. Hoerlein, R. Costa, G. Schiller, K.A. Friedrich, Sulfur poisoning of electrochemical reformate conversion on nickel/gadolinium-doped ceria electrodes, ACS Catal. 7 (11) (2017) 7760–7771, https://doi.org/10.1021/acscatal.7b02177.
[25] M. Riegraf, F. Han, N. Sata, R. Costa, Intercalation of thin film Gd-doped ceria barrier layers in electrolyte supported solid oxide cells: Physico-chemical aspects, ACS Appl. Mater. Interfaces 13 (31) (2021) 37239–37251, https://doi.org/10.1021/acsami.1c11175.
[26] M. Riegraf, R. Costa, G. Schiller, K.A. Friedrich, S. Dierickx, A. Weber, Electrochemical impedance analysis of symmetrical Ni/gadolinium-doped ceria (CGO10) electrodes in electrolyte-supported solid oxide cells, J. Electrochem. Soc. 166 (13) (2019) F865–F872, https://doi.org/10.1149/2.0051913jes.
[27] C. Grosselindemann, N. Russner, S. Dierickx, F. Wankmüller, A. Weber, Deconvolution of gas diffusion polarization in Ni/gadolinium-doped ceria fuel

electrodes, J. Electrochem. Soc. 168 (12) (2021) 124506, https://doi.org/10.1149/1945-7111/ac3d02.
[28] S. Primdahl, Y.L. Liu, Ni catalyst for hydrogen conversion in Gadolinia-doped ceria anodes for solid oxide fuel cells, J. Electrochem. Soc. 149 (11) (2002) A1466–A1472, https://doi.org/10.1149/1.1514234.
[29] N. Jacobson, D. Myers, E. Opila, E. Copland, Interactions of water vapor with oxides at elevated temperatures, J. Phys. Chem. Solids 66 (2–4) (2005) 471–478.
[30] P.S. Gentile, S.W. Sofie, C.F. Key, R.J. Smith, Silicon volatility from alumina and Aluminosilicates under solid oxide fuel cell operating conditions, Int. J. Appl. Ceram. Technol. 9 (6) (2012) 1035–1048, https://doi.org/10.1111/j.1744-7402.2011.02688.x.
[31] H. Van Hal, H. Hintzen, Compound formation in the Ce2O3-SiO2 system, J. Alloys Compd. 179 (1–2) (1992) 77–85.
[32] A.C. Strzelecki, K. Kriegsman, P. Estevenon, V. Goncharov, J. Bai, S. Szenknect, A. Mesbah, D. Wu, J.S. McCloy, N. Dacheux, High-temperature thermodynamics of cerium silicates, A-Ce2Si2O7, and Ce4. 67 (SiO4) 3O, ACS Earth Space Chem. 4 (11) (2020) 2129–2143.
[33] M. Santoro, F. Gorelli, J. Haines, O. Cambon, C. Levelut, G. Garbarino, Silicon carbonate phase formed from carbon dioxide and silica under pressure, Proc. Natl. Acad. Sci. 108 (19) (2011) 7689–7692, https://doi.org/10.1073/pnas.1019691108.
[34] Y.-M. Park, K.-M. Yeon, C.-h. Park, Silica treatment technologies in reverse osmosis for industrial desalination: a review, Environ. Eng. Res. 25 (6) (2020) 819–829, https://doi.org/10.4491/eer.2019.353.
[35] W.G. Bessler, S. Gewies, Gas concentration impedance of solid oxide fuel cell anodes, J. Electrochem. Soc. 154 (6) (2007) B548–B559.
[36] J. Kondoh, T. Kawashima, S. Kikuchi, Y. Tomii, Y. Ito, Effect of aging on Yttria-stabilized zirconia: I. A study of its electrochemical properties, J. Electrochem. Soc. 145 (5) (1998) 1527–1536, https://doi.org/10.1149/1.1838515.
[37] A. Müller, A. Weber, E. Ivers-Tiffée, Degradation of zirconia electrolytes, Proceedings of the sixth European Solid Oxide Fuel Cell Forum 28 (2004) 1231–1238.
[38] F.T. Ciacchi, S.P.S. Badwal, The system Y2O3-Sc2O3-ZrO2: phase stability and ionic conductivity studies, J. Eur. Ceram. Soc. 7 (3) (1991) 197–206, https://doi.org/10.1016/0955-2219(91)90037-Z.
[39] C. Geipel, K. Hauptmeier, K. Herbrig, F. Mittmann, M. Münch, M. Pötschke, L. Reichel, T. Strohbach, T. Seidel, A. Surrey, Stack development and industrial scale-up, ECS Trans. 91 (1) (2019) 123.
[40] M.P. Hoerlein, M. Riegraf, R. Costa, G. Schiller, K.A. Friedrich, A parameter study of solid oxide electrolysis cell degradation: microstructural changes of the fuel electrode, Electrochim. Acta 276 (2018) 162–175, https://doi.org/10.1016/j.electacta.2018.04.170.
[41] J. Aicart, A. Surrey, L. Champelovier, K. Henault, C. Geipel, O. Posdziech, J. Mougin, Benchmark study of performances and durability between different stack technologies for high temperature electrolysis, Fuel Cells 23 (6) (2023) 463–473, https://doi.org/10.1002/fuce.202300028.
[42] J. Aicart, L. Tallobre, A. Surrey, B. Gervasoni, C. Geipel, H. Fontaine, S. Desousanobre, J. Mougin, Lifespan evaluation of two 30-cell electrolyte-supported stacks for hydrogen production by high temperature electrolysis, Int. J. Hydrog. Energy 60 (2024) 531–539.
[43] S. GmbH, Final Project Report - 'Verbundvorhaben P2X: Erforschung, Validierung und Implementierung von Power-to-X Konzepten - Teilvorhaben Q'. (2020), https://doi.org/10.2314/KXP:1736046187.
[44] A. Léon, A. Micero, B. Ludwig, A. Brisse, Effect of scaling-up on the performance and degradation of long-term operated electrolyte supported solid oxide cell, stack and module in electrolysis mode, J. Power Sources 510 (2021) 230346, https://doi.org/10.1016/j.jpowsour.2021.230346.
[45] M. Riegraf, D.-M. Amaya-Dueñas, N. Sata, K.A. Friedrich, R. Costa, Performance and limitations of nickel-doped chromite anodes for solid oxide fuel cells (SOFC), ChemSusChem 14 (2021) 1–14, https://doi.org/10.1002/cssc.202100330.
[46] T. Zhang, M.D. Amiridis, Hydrogen production via the direct cracking of methane over silica-supported nickel catalysts, Appl. Catal. A Gen. 167 (2) (1998) 161–172, https://doi.org/10.1016/S0926-860X(97)00143-9.
[47] Y. Liu, C. Jiao, Microstructure degradation of an anode/electrolyte interface in SOFC studied by transmission electron microscopy, Solid State Ionics 176 (5–6) (2005) 435–442.
[48] A. Staerz, H.G. Seo, T. Defferriere, H.L. Tuller, Silica: ubiquitous poison of metal oxide interfaces, J. Mater. Chem. A 10 (6) (2022) 2618–2636.
[49] C. Nicollet, C. Toparli, G.F. Harrington, T. Defferriere, B. Yildiz, H.L. Tuller, Acidity of surface-infiltrated binary oxides as a sensitive descriptor of oxygen exchange kinetics in mixed conducting oxides, Nat. Catal. 3 (11) (2020) 913–920.
[50] F. Straub, H. Grabowski, Silica deposition in steam turbines, Trans. Am. Soc. Mech. Eng. 67 (5) (1945) 309–314.